Brief communication

Single-nucleus mRNA-sequencing reveals dynamics of lipogenic and thermogenic adipocyte populations in murine brown adipose tissue in response to cold exposure

Janina Behrens [1], Tongtong Wang [2], Christoph Kilian [3], Anna Worthmann [1], Joerg Heeren [1], Lorenz Adlung [3, 4,*], Ludger Scheja [1,*]

[1] Department of Biochemistry and Molecular Cell Biology, University Medical Center Hamburg-Eppendorf, Hamburg, Germany

[2] Laboratory of Translational Nutrition Biology, Institute of Food, Nutrition and Health, Department of Health Sciences and Technology ETH Zürich, Schwerzenbach, Switzerland

[3] I. Department of Medicine, University Medical Center Hamburg-Eppendorf (UKE), Hamburg, Germany

[4] Center for Translational Immunology (HCTI) and Center for Biomedical AI (bAIome), University Medical Center Hamburg-Eppendorf (UKE), Hamburg, Germany

*Corresponding authors: Department of Biochemistry and Molecular Cell Biology, I. Department of Medicine, University Medical Center Hamburg-Eppendorf (UKE), Martinistraße 52, 20246 Hamburg, Germany. Email: l.scheja@uke.de, l.adlung@uke.de

ABSTRACT

Brown adipose tissue (BAT) comprises a heterogeneous population of adipocytes and non-adipocyte cell types. To characterize these cellular subpopulations and their adaptation to cold, we performed single-nucleus mRNA-sequencing (snRNA-seq) on interscapular BAT from mice maintained at room temperature or exposed to acute (24h, AC) or chronic (10 days, CC) cold (6°C). To investigate the role of the *de novo* lipogenesis (DNL)-regulating transcription factor carbohydrate response element-binding protein (ChREBP), we analyzed control and brown adipocyte-specific ChREBP knockout mice. We identified different cell populations, including seven brown adipocyte subtypes with distinct metabolic profiles. One of them highly expressed ChREBP and DNL enzymes. Notably, these lipogenic adipocytes were highly sensitive to acute cold exposure, showing a marked depletion in BAT of control mice that was compensated by other brown adipocyte subtypes maintaining DNL. Chronic cold exposure resulted in an expansion of basal brown adipocytes and adipocytes putatively derived from stromal and endothelial precursors. In ChREBP-deficient mice, lipogenic adipocytes were almost absent under all conditions, identifying the transcription factor as a key determinant of this adipocyte subtype. Pathway and cell-cell interaction analyses implicated a Wnt-ChREBP axis in the maintenance of lipogenic adipocytes, with Wnt ligands from stromal and muscle cells providing instructive cues. Our findings provide a comprehensive atlas of BAT cellular heterogeneity and reveal a critical role for ChREBP in lipogenic adipocyte identity, with implications for BAT plasticity and metabolic function.

1. INTRODUCTION

Brown adipose tissue (BAT) is a thermogenic organ designed to maintain core body temperature during cold stress. When activated under such condition, brown adipocytes produce heat by oxidizing large amounts of energy substrates without a corresponding synthesis of ATP [1]. This process, known as non-shivering thermogenesis, relies primarily on a proton shunt in the inner mitochondrial membrane mediated by uncoupling protein-1 (UCP1) [2]. In addition, UCP1-independent futile cycles such as creatine phosphate cycling have been shown to contribute to BAT thermogenesis [3–5]. Brown adipocytes are activated largely by norepinephrine released from sympathetic nerve endings [6], but also by other hormonal triggers [7], that ultimately stimulate lipases and thus the release of fatty acids from lipid droplets [8,9]. Next to serving as fuel, the lipolysis-derived fatty acids allosterically activate UCP1 [10]. To sustain its extremely high metabolic rate, activated BAT takes up high amounts of energy substrates from the circulation, including fatty acids released by lipoprotein lipase from triglyceride-rich lipoproteins [11], free fatty acids originating from lipolysis in white adipose tissue (WAT) [12,13], glucose [14], amino acids [15,16] and acylcarnitines [12].

A characteristic feature of BAT intermediary metabolism is that, for reasons not well understood, it exhibits a high capacity for *de novo* lipogenesis (DNL), the generation of fatty acids from non-lipid precursors [17–20]. In the context of high fatty acid oxidation within activated BAT, high DNL may serve heat production through futile cycling [19]. Alternatively, it may be required for producing intracellular membranes needed for the expansion of mitochondria [21,22]; and possibly other cellular organelles in response to cold stimulation. Also, DNL may be essential for cell proliferation which is a crucial process taking place during the adaptation of BAT to prolonged cold exposure. Proliferation involves not only endothelial cells needed for expansion of the capillaries [21], but also differentiation of new brown adipocytes that originate from adipose stromal cells (ASCs) [23–25], vascular smooth muscle cells (VSMCs) [26]; and endothelial cell-derived precursors [27]. Together, the proliferation and growth processes result in an enlarged BAT organ with increased thermogenic capacity and an expanded capillary network.

DNL enzymes are expressed at much higher level in the active BAT of mice kept at room temperature than in the inactive BAT of mice housed at 30°C (thermoneutrality) [17], further supporting an involvement of this metabolic pathway in BAT thermogenesis. Notably, a recent transcriptomic study employing single nuclei RNA-sequencing (snRNA-seq) methodology identified a small adipocyte subset in murine BAT with high expression of DNL genes [28]. In this investigation, mice housed under thermoneutrality were repeatedly exposed to short periods (8 h) of cold. It was found that the lipogenic adipocyte cluster correlates in size with

BAT activation state, and evidence was provided that these cells are important for thermogenic function in this particular cold exposure regimen.

To further investigate the role of DNL in BAT activation and its impact on cellular composition, we performed snRNA-seq of BAT from mice kept at room temperature and from mice acutely (24 h) or chronically (10 days) exposed to cold (6°C). Knockout of the lipogenic transcription factor carbohydrate response element-binding protein (ChREBP, encoded by *Mlxipl*), was used to study the impact of DNL on metabolic and regulatory functions of adipocyte subtypes. We provide an atlas of 21 distinct BAT adipocyte and non-adipocyte cell types. The adipocyte subtypes exhibit metabolic specialization and, importantly, pronounced changes in frequency upon acute and chronic cold exposure, respectively. We confirm the presence of a distinct lipogenic brown adipocyte. Surprisingly, acute cold exposure transiently depletes lipogenic adipocytes from BAT, while their DNL function is compensated by another subset of brown adipocytes. Of note, ChREBP knockout depletes lipogenic adipocytes from BAT irrespective of housing temperature without affecting energy homeostasis under cold stress in these mice, indicating that the loss of these adipocytes (and of DNL) can be compensated by the BAT organ.

2. RESULTS

2. 1. Identification of distinct clusters of adipocytes and other cell types in BAT by single nuclei RNA-seq

Brown adipocyte-specific ChREBP knockout were generated by crossing mice with a floxed exon1a in the *Mlxipl* gene [29] with Ucp1-Cre mice [30], as previously described [31]. These ChREBP$^{flox/flox}$ Ucp1-Cre+ (Cre+) mice and ChREBP-expressing control (Cre-) mice were studied under various conditions of BAT activation. Housing at room temperature (22°C, RT) was chosen as a control condition when BAT is mildly activated [17]. Cold-exposure (6°C) was carried out for 1 day (acute cold), as an early stage when proliferative processes of BAT adaptation are not yet taking place [24,32], or for 10 days (chronic cold) when BAT is fully expanded [32]. Compared to Cre- mice, Cre+ mice showed a profound reduction of the targeted isoform, ChREBPα (*Mlxipl*, isoform 1), at mRNA (Figure 1A) and protein level (Figure 1B) under all conditions. The other, shorter isoform ChREBPβ (*Mlxipl*, isoform 2) was also strongly reduced [33] at mRNA level (Figure 1A), however, could not be detected at protein level.

To study the cellular composition of BAT, snRNA-seq was performed in Cre- and Cre+ mice, using the 10X Genomics Chromium system, as described previously [34]. BAT from 3-4 mice were pooled per sample. After quality control (see Methods section), 36,611 nuclei were

116 retrieved in total, including both genotypes and all three housing conditions. A total of 21
117 cellular clusters were identified using this complete data set (Figure 1C) and annotated in a
118 semi-supervised manner through marker genes for the respective cell types described in the
119 literature. Seven clusters could be annotated as adipocytes and were characterized by a high
120 average expression of adipocyte markers such as *Lipe*, *Plin1* and *Pparg* (Figure S1A).
121 Confirming the identity of these clusters as adipocytes, they exhibited a high gene expression
122 score based on genes previously found to identify brown and white adipocytes [35],
123 respectively (Figure 1D).

124 The largest adipocyte cluster (hereafter referred to as **basal brown adipocytes**) was found to
125 express thermogenic transcription factors and coactivators such as *Prdm16* [36], *Esrrg* [37,38],
126 *Ppargc1a [22]* and *Ppargc1b* [39] (Figure 1E). Also, they express high levels of other brown
127 fat markers such as *Ucp1* [2], *Cidea* [40] and *Dio2* [41] (Figure 1E), and have a high brown
128 adipocyte score (Figure 1D). The second-largest cell cluster consisted of brown adipocytes
129 that were distinguished from the basal ones by higher average expression of genes important
130 for handling high quantities of fatty acids, namely the fatty acid-binding protein *Fabp4* and the
131 fatty acid desaturase *Scd1* (Figure 1E). Of note, pathway analysis of marker genes indicated
132 high oxidative phosphorylation capacity of those cells (KEGG [42] pathway mmu10090; p adj.
133 = 5.8e-40, Figure S1B). Thus, the cells were dubbed OXPHOS-high brown adipocytes
134 (hereafter referred to as **OXPHOS-high adipocytes**). Of note, mitochondrially encoded
135 OXPHOS genes were also enriched in this adipocyte class (Figure S1B), suggesting higher
136 association of mitochondria with the nuclei extracted from these cells.

137 The third-largest adipocyte cluster was characterized by relatively low expression of *Ucp1* but
138 included cells with high expression of the white adipocyte markers *Retn* and *Lep* [26] as well
139 as *Adipoq* (Figure 1E). Moreover, they were distinguished from the other adipocyte clusters by
140 a high white adipocyte score (Figure 1D). High average expression of *Cyp2e1*, *Slc7a10* and
141 *Aldh1a1* (Figure 1E) identified these cells as **white-like adipocytes** previously found in murine
142 BAT [28,34] that were shown to have more white adipocyte-typical properties and suppress
143 thermogenic responses in other BAT adipocytes [34]. Surprisingly, some of the white-like
144 adipocytes expressed considerable levels of *Slc2a3*, coding for the brain-type glucose
145 transporter GLUT3 [43] that is not well-studied in adipocytes, however, was recently reported
146 to be expressed in bone marrow adipocytes [44]. Also, compared to all other clusters they
147 expressed the highest levels of thyroid-stimulating hormone receptor (*Tshr*), a $G_{\alpha S}$-coupling
148 receptor previously reported to confer brown adipocyte activation [45–47] (Figure 1E).
149 Consistent with *Slc2a3* and *Tshr* as white adipocyte markers, we observed considerably higher
150 expression of these genes in WAT depots compared to BAT in a separate cohort of wild type
151 mice (Figure S1C).

152 Yet another minor adipocyte cluster was similar to basal adipocytes, however, expressed DNL
153 genes (*Acaca*, *Fasn*) and *Mlxipl* at a higher level (Figure 1E). This adipocyte sub-cluster
154 corresponds to lipogenic brown adipocytes (hereafter referred to as **lipogenic adipocytes**)
155 recently described in murine BAT by Lundgren *et al*. [28]. Gene expression in these cells
156 exhibited strong correlation with those identified by Lundgren *et al.* (Pearson's r = 0.93; p<2.2e-
157 16; Figure 2A). Furthermore, this cluster is enriched in the transcription factor *Bhlhe40* (Figure
158 1E) recently described as a marker gene for a DNL-high adipocyte subpopulation in inguinal
159 WAT [48]. Notably, the gene most highly enriched in lipogenic adipocytes in the current study
160 was *Ttc25*, for example when compared to the similar basal brown adipocytes (Figure 2B).
161 This gene encodes for a protein important for the assembly of motile cilia [49] with unknown
162 function in adipocytes. Of note, *Ttc25* was a more specific marker of lipogenic adipocytes than
163 DNL enzymes such as *Fasn* (Figure 2C). To get an indication about the functional role of *Ttc25*
164 in lipogenic adipocytes, we performed a correlation analysis. Genes highly correlating with
165 *Ttc25* in lipogenic adipocytes (Figure 2D) were subjected to gene ontology (GO) term analysis
166 and yielded biological processes related to fatty acid metabolism and thermogenesis (Figure
167 2E), indicating a strong link of this gene to fatty acid metabolization and BAT heat generation.

168 Additional brown adipocyte clusters shared gene signatures with skeletal muscle cells, stromal
169 cells and endothelial cells, respectively. One of them expressed high levels of muscle proteins
170 such as *Myh2*, *Myh7*, *Tnnc2*, *Tnni2* and *Ttn* (Figure 1E) but was otherwise very similar to
171 OXPHOS-high adipocytes. These cells might mediate contractile processes previously shown
172 to participate in BAT activation [50] and were, therefore, tentatively identified as contractile
173 brown adipocytes (hereafter referred to as **contractile adipocytes**). Two *bona fide* muscle
174 fiber clusters were also observed, **fast fibers**, identified by high expression of typical markers
175 such as *Myh1*, *Myh2*, *Myh4*, *Tnnc2*, *Tnni2*, *Tnnt3* [51,52] and **slow fibers**, highly expressing
176 the typical markers *Myh7*, *Tnnc1*, *Tnni1* and *Tnnt1* [51] (Figure S1D).

177 Among endothelial cells, capillary, arterial and venous clusters could be distinguished. All
178 clusters were characterized by prominent expression of the general endothelial cell markers
179 *Pecam1* and *Cdh5* (Figure S1E). **Capillary endothelial cells** expressed high levels of genes
180 involved in trans-endothelial lipid processing and transport, including *Gpihbp1* [53], *Cd36*
181 [54,55] and *Fabp4* [56,57]. **Arterial endothelial cells** were defined by high expression of the
182 artery markers *Bmx* [58], *Fbln5*, and *Cytl1* [59]. **Venous endothelial cells** shared with arterial
183 ones expression of the large vessel markers *Vwf* and *Vcam1* [59]. They were identified as
184 venous endothelial cells based on expressing at high level the markers *Gm5127*, *Ephb4*, *Nrp2*,
185 *Nr2f2* [60]. Notably, a brown adipocyte cluster expressing brown adipocyte markers including
186 *Ucp1*, *Cidea*, *Plin1* and *Prdm16* (Figure 1E) also exhibited a weaker yet clear endothelial cell
187 signature (Figure S1E). These cells were interpreted as being brown adipocytes differentiated

188 from endothelial cells-derived precursors (hereafter referred to as **endothelium-derived**
189 **adipocytes**).

190 Three stromal cells clusters were identified by expression of the general stromal cell markers
191 *Pdgfra*, *Col1a1* and *Dcn* [25] (Figure S1F). These were found to largely correspond to three
192 stromal cell clusters (ASC1-ASC3) identified in a previous single cell RNA-seq study
193 investigating BAT stromal-vascular fraction [25]. Consistent with that study, **stromal cells type**
194 **1** were enriched in ASC1 markers in *Col5a3* and *Bmper*, **stromal cells type 2** in the ASC2
195 markers *Pi16*, *Dpp4* and *Fbn1*, and **stromal cells type 3** in the ASC3 markers *Fbln1* and
196 *Gdf10* (Figure S1F). Notably, a minor cluster of brown adipocytes showed a signature related
197 to the three stromal cell clusters (Figure S1F). These cells were interpreted to be brown
198 adipocytes differentiated from stromal cells (hereafter referred to as **stroma-derived**
199 **adipocytes**).

200 Other cell types identified in the analysis by typical marker genes (shown in brackets)
201 encompassed myeloid cells (**MonDC**) that were enriched in monocyte/macrophage and
202 dendritic cell marker genes [25] (e.g. *Mctp1*, *Mrc1*, *Adgre1*, *Itgam;* Figure S1G). Moreover,
203 mural cells including **smooth muscle cells** [26] (e.g. *Acta2*, *Myh11*, *Mylk*, *Trpv1*; Figure S1G)
204 and **pericytes** [59] (e.g. *Pdgfrb*, *Rgs5*, *Kcnj8*; Figure S1G) were identified. The smallest cluster
205 included **lymphocytes** [61,62] (e.g. *Cd3e*, *Skap1*, *Itk*; Figure S1G), as well as glia cells
206 including cells similar to non-myelinating **satellite glia** [63,64] (e.g. *L1cam*, *Zfp536*; Figure
207 S1G) and **Schwann cells** [64,65] (e.g. *Mbp*, *Mpz*; Figure S1G).

208 **2.2. Changes in frequency of adipocyte clusters and metabolic/thermogenic pathway**
209 **enrichment during chronic cold adaptation**

210 Adipocytes contributed ca. 60% of all BAT nuclei (Figure S2). To understand the impact of
211 long-term BAT activation on adipocyte subtypes and their metabolic adaptation, the relative
212 sizes of the adipocyte clusters (Supplemental Table 2) were studied in BAT from Cre- mice
213 chronically exposed to cold (10 days 6°C). Compared to Cre- mice housed at room
214 temperature the fraction of basal brown adipocytes increased after chronic cold at the expense
215 of OXPHOS-high adipocytes and constituted 59% of all adipocytes during chronic cold (Figure
216 3A). Stroma- and endothelium-derived adipocytes contributed 7.2% to total adipocyte nuclei
217 at room temperature but increased to 9.7% after chronic cold exposure, probably reflecting
218 enhanced adipocyte differentiation as part of BAT adaptation [23–27] (Figure 3A). In contrast,
219 the proportion of white-like adipocytes dropped during cold adaptation from 11.6% to 7%,
220 which is consistent with the reported negative correlation of this anti-thermogenic subclass
221 with BAT activation state [28,34] (Figure 3A). The number of lipogenic adipocytes increased
222 moderately after chronic cold and constituted 14.4% under that condition (Figure 3A), which is

223 consistent with the proposed role of these adipocytes in providing other brown adipocytes with
224 acylcarnitines as energy substrate when BAT is chronically activated [28].

225 Next, we sought to understand the contribution of the adipocyte subsets to heat-generating
226 energy dissipation, and how they respond to cold exposure. For this purpose, we curated a list
227 of genes representing the oxidative branches of metabolism required to produce energy from
228 fatty acids and glucose (Supplemental Table 1), the two major energy substrates in BAT [13].
229 Also included in this list were DNL and mediators of non-shivering thermogenesis. Calculated
230 gene scores based on average expression were then used to compare the enrichment of the
231 metabolic pathways and processes among the various adipocyte clusters (relative to basal
232 brown adipocytes) at baseline and after the cold exposure regimens (Figure 3B). At room
233 temperature, the pathways mediating oxidation of glucose (glycolysis, pyruvate
234 dehydrogenase, citric acid cycle) and the conversion of glucose into fatty acids (pentose
235 phosphate pathway, DNL) exhibited higher expression in basal, lipogenic, endothelium-
236 derived and stroma-derived brown adipocytes compared to OXPHOS-high, white-like and
237 contractile adipocytes (Figure 3B). Similarly, oxidative metabolism of fatty acids (fatty acid
238 transport, carnitine shuttle, beta-oxidation) was enriched in the basal and endothelium-derived
239 and stroma-derived brown adipocytes, particularly in comparison to OXPHOS-high, white-like
240 and contractile adipocytes (Figure 3B). OXPHOS genes and fatty acid binding proteins showed
241 highest expression in OXPHOS-high and contractile brown adipocytes at room temperature
242 (Figure 3B). Under chronic cold exposure, the oxidative branches of energy metabolism were
243 generally upregulated compared to room temperature in the brown adipocyte clusters, most
244 strongly the OXPHOS genes. Of note, DNL genes went up in most adipocytes except for
245 lipogenic adipocytes under chronic cold exposure (Figure 3B). Overall, these data indicate a
246 general upregulation of oxidative capacity of brown adipocytes as an adaptation to sustained
247 thermogenic demand, while differences in metabolic pathways between adipocyte subtypes
248 present at baseline tend to become smaller.

249 Among the non-shivering thermogenesis pathways, *Ucp1* showed highest enrichment in basal
250 brown adipocytes at room temperature, however was highly induced in OXPHOS-high and
251 contractile brown adipocytes after chronic cold exposure (Figure 3B). Genes of calcium cycling
252 were enriched in the contractile brown adipocyte cluster, however, showed overall no cold-
253 dependent regulation, whereas genes of triglyceride cycling were lower in white-like,
254 OXPHOS-high and contractile adipocytes and showed moderate induction upon chronic cold
255 (Figure 3B). Of note, creatine cycling did not show enrichment in any brown adipocyte cluster
256 and was generally but moderately upregulated upon cold exposure (Figure 3B).

257 **2.3. Increase in OXPHOS-high but decrease in white-like and lipogenic adipocytes**
258 **during acute adaptation to cold environment**

259 To investigate how cold exposure acutely (24 h 6°C) influences the relative abundance of the
260 adipocyte subtypes, the fractions of each adipocyte cluster under this condition were compared
261 with those at room temperature (summarized in Supplemental Table 2). Basal, stroma- and
262 endothelium-derived adipocytes did not change clearly after acute cold exposure (Figure 3A).
263 In contrast, acute cold exposure caused a doubling in the number of OXPHOS-high and
264 contractile adipocytes (Figure 3A). The higher relative fraction of OXPHOS-high adipocytes
265 was paralleled by markedly increased expression of *Ucp1*, OXPHOS genes, and fatty acid
266 binding proteins in these cells (Figure 3B). Of note, key OXPHOS regulators (*Ppgrc1a*, *Tfam*)
267 were strongly induced in all other brown adipocytes (Figure 3B). Moreover, a general induction
268 of *Ucp1* and also of the pathways of fuel oxidation was observed throughout all brown
269 adipocyte clusters (Figure 3B).

270 Surprisingly, the numbers of both lipogenic and white-like adipocytes dropped markedly during
271 acute cold exposure (Figure 3A). We reasoned that an explanation for this drop upon acute
272 cold exposure could have been more apoptosis. However, an expression score of apoptosis
273 signature genes (from WikiPathways [66] WP1254; Supplemental Table 1) was found to
274 decrease rather than increase in these cells under cold exposure (Figure 3C), a finding that is
275 in line with previous research observing lower apoptosis in BAT after one day of cold exposure
276 [67]. To corroborate whether the sharp drop in the number of lipogenic adipocytes upon acute
277 cold exposure causes a transient downregulation of DNL in BAT as a whole, we investigated
278 the expression of two key DNL enzymes, *Acaca* and *Fasn*, on a pseudobulk level. Interestingly,
279 both enzymes exhibited only a slight reduction after acute cold exposure at the total organ
280 level (Figure 3D). To confirm this finding, we performed qPCR of BAT from an independent
281 cohort of mice and found significantly higher levels after chronic cold exposure, but only a
282 slight, non-significant reduction of *Acaca* and *Fasn* expression under acute cold exposure
283 (Figure 3E). We reasoned that DNL is thus carried out by another adipocyte subset under
284 these conditions. To investigate a potential compensation mechanism, we looked at the total
285 transcript number (aggregated expression) of the DNL enzymes across the different adipocyte
286 populations in our snRNA-seq data set (Figure 3F). Notably, basal adipocytes have the highest
287 transcript numbers and thus contribution to total BAT expression of the two DNL enzymes
288 under acute cold exposure (Figure 3F). To check for a potential trans-differentiation from
289 lipogenic to basal adipocytes explaining this observed compensatory mechanism of DNL under
290 acute cold, we performed trajectory analysis by RNA velocity [68], a method that estimates
291 future gene expression by comparing spliced versus un-spliced transcript variants. However,
292 based on our snRNA-seq data there was no dynamics inferred between those two clusters, at
293 least at this time point of acute cold exposure (Figure 3G), nor at chronic cold (Figure 3H).

294 Taken together, cold exposure for one day does not only lead to an induction of pathways
295 necessary to cope with increased thermogenic demand. It also triggers pronounced shifts in
296 cell identities toward the presumably very thermogenic OXPHOS-high adipocytes and away
297 from the *Ucp1*-low lipogenic and white-like adipocytes.

298 **2.4. ChREBP is essential for lipogenic adipocyte identity but not essential for BAT**
299 **thermogenic function**

300 Previously, we demonstrated that ChREBP is the dominant transcription factor regulating DNL
301 in BAT [31]. To better understand the regulatory fine-tuning of BAT DNL under cold, we
302 analyzed the tissue-specific ChREBP (*Mlxipl*) knockout (Cre+) mice (Figure 1A,B). As
303 expected, loss of ChREBP led to significant reduction of the targets *Fasn* and *Acaca* on total
304 tissue RNA and protein level (Figure 4A, B). This result was confirmed by pseudobulk analysis
305 in the snRNA-seq data set (Figure 4C). On single nucleus level, brown adipocytes from Cre+
306 mice, exhibited reduced expression of *Mlxipl* and DNL genes, whereas expression by white-
307 like adipocytes was almost unchanged (Figure S3), explained by low Ucp1-promotor activity
308 in the latter adipocyte subtype. Importantly, the DNL-derived fatty acids myristic (14:0) and
309 palmitic acid (16:0) were relatively depleted in Cre+ compared to Cre- BAT under all three
310 housing conditions (Figure 4D). This indicated that ChREBP-dependent DNL has an impact
311 on BAT lipid homeostasis even in highly activated BAT, which takes up very high quantities of
312 fatty acids from the circulation [11,13]. To test the functional relevance of ChREBP for BAT
313 thermogenesis, we compared brown adipocyte scores under the various conditions and found
314 a higher score in adipocytes from Cre+ compared to Cre- mice at room temperature, whereas
315 brown adipocyte scores were lower in Cre+ under cold exposure (Figure S4A). However, this
316 gene expression difference did not translate to a major thermogenic phenotype, as shown by
317 indirect calorimetry of Cre- and Cre+ mice. Cre+ versus Cre- mice housed at room temperature
318 or under cold exposure displayed no difference in energy expenditure (Figure S4B).

319 Next, we assessed the impact of ChREBP deficiency on the sizes of the brown adipocyte
320 clusters. The proportion of OXPHOS-high adipocytes was higher in Cre+ compared to Cre-
321 mice at room temperature and after chronic cold (Figure 4E), which might explain the lack of
322 phenotype regarding energy expenditure. Surprisingly, the number of lipogenic adipocytes was
323 very low under all conditions in Cre+ mice (Figure 4E), demonstrating that ChREBP is an
324 essential factor for establishing lipogenic adipocyte identity. This notion was supported by the
325 observation that the few remaining lipogenic adipocytes in Cre+ animals showed strong
326 expression of ChREBP and its target genes such as *Acaca*, *Fasn* (Figure S3), possibly
327 representing cells in which knockout by the transgenic Ucp1-Cre had failed.

328 **2.5. The functional identity of BAT lipogenic adipocytes correlates with Wnt signaling**

329 As the presence of lipogenic adipocytes was strongly dependent on ChREBP irrespective of
330 housing temperatures, we sought to identify signaling pathways that might explain the
331 functional dependency on ChREBP. To this end, we performed PROGENy pathway analysis
332 [69] in lipogenic adipocytes. Among the pathways investigated, Wnt signaling was found to be
333 the predominantly active in lipogenic adipocytes (Figure 4F). Notably, the Wnt PROGENy
334 score showed a ChREBP-dependent effect in lipogenic adipocytes (Figure 4G), despite *Mlxipl*
335 (ChREBP) not being included in the gene set fed into the algorithm, suggesting that genetic
336 ablation of ChREBP affects the Wnt signaling in lipogenic adipocytes. The low number of
337 lipogenic adipocytes of Cre- animals under acute cold exposure (Figure 4E) may be due to a
338 reduction of Wnt ligands in after acute cold compared to room temperature and chronic cold.
339 Indeed, we observed lower aggregated Wnt expression in BAT at acute cold compared to room
340 temperature and chronic cold (Figure 4H). To investigate, whether Wnt signaling can be
341 associated with brown adipocyte functional identity in lipogenic adipocytes, we correlated the
342 Wnt PROGENy score to the brown adipocyte score for this adipocyte subtype (Figure S4C).
343 While we found a significant positive correlation for the cells coming from the Cre- mice, no
344 significant correlation was identified for the lipogenic adipocytes from Cre+ animals, which
345 suggests that Wnt signaling and brown adipocyte identity were uncoupled upon genetic
346 ablation of ChREBP and subsequent loss of DNL function of lipogenic adipocytes (Figure
347 S4C).

348 To identify the cellular sources of Wnt ligands, which seemed to provide functionally relevant
349 signaling cues to lipogenic adipocytes in BAT of Cre- mice, cell-cell interaction analysis was
350 performed using LIANA [70]. We found *Wnt5a* and *Wnt5b*, expressed by fast muscle fibers,
351 slow muscle fibers, and stroma-derived brown adipocyte progenitors to act on lipogenic
352 adipocytes (Figure 4I). Of note, a total of 152 significant (adjusted $p < 0.05$) cell-cell interactions
353 were identified between these four cell populations (Figure 4J), suggesting the presence of a
354 cell-type instructive signaling network that involves Wnt and other signaling molecules.

355 Taken together, our results demonstrate that ChREBP is essential for maintaining the identity
356 of lipogenic brown adipocytes, which is seemingly instructed through Wnt signaling possibly
357 originating from muscle cells and newly differentiating adipocytes within BAT.

358

359 **3. DISCUSSION**

360 In the current study, we employed snRNA-seq to generate a comprehensive atlas of murine
361 BAT cell types at room temperature and under cold exposure. In our data analysis, we focused
362 on adipocyte subtypes to find out how they respond to acute or chronic cold exposure, so they
363 eventually confer adaptation of BAT to increased thermogenic demand. Using the largest cell

364 cluster, basal brown adipocytes, as a reference, the other adipocyte clusters were assigned
365 phenotypes and identities according to their gene expression pattern. OXPHOS-high
366 adipocytes and the putatively contractile adipocytes are characterized by a high capacity to
367 dissipate energy in an UCP1-dependent manner through the oxidation of fatty acids. Both
368 clusters more than doubled in cell numbers after one day of cold exposure, a process that
369 might serve to swiftly expand the heat generation capacity of BAT under this condition when
370 BAT as an organ has not yet expanded [24,32]. Conversely, the white-like adipocytes,
371 described in two previous studies [28,34], declined profoundly already after one day of cold
372 exposure, a process that is physiologically consistent with their proposed role as negative
373 regulators of thermogenesis [34]. The marked changes in the frequencies of OXPHOS-high,
374 contractile, white-like and also lipogenic adipocytes upon acute cold exposure at a time point
375 when both proliferation [24,32] and apoptosis [67] are low, suggest that they are not caused
376 by classical trans-differentiation or cell death. Rather, they likely reflect functional adaptation
377 of the cell states to altered thermogenic demand. Our findings are in line with the dynamic
378 transcriptional heterogeneity reported previously in brown adipocytes [53,71], and they extend
379 the notion of highly plastic, responsive brown adipocyte states [72].

380 In the current study, we confirmed the presence in BAT of a distinct lipogenic adipocyte
381 subtype that was recently described by Lundgren *et al.* [28]. We further characterized this cell
382 type by identifying *Ttc25* as a highly specific marker of this adipocyte subpopulation. *Ttc25*
383 encodes for a protein mediating the assembly of motile cilia, as exemplified by the phenotypes
384 of *Ttc25*-deficient mice [73] and humans [73,74]. Notably, primary cilia have been shown to
385 mediate adipogenesis, for example through sensing of their microenvironment [75] and one
386 might speculate that *Ttc25* also acts on these specialized cilia, thereby supporting signaling
387 events that confer the lipogenic phenotype. Of note, pathway analysis demonstrated that
388 genes highly correlating with *Ttc25* exhibit a strong link to fatty acid metabolism and adaptive
389 thermogenesis. This observation is in consistent with the proposed role of the lipogenic
390 adipocytes in providing fatty acid carnitine esters as fuel to other brown adipocytes [28].
391 Whether *Ttc25* plays a regulatory role in metabolism or in the functional identity of lipogenic
392 adipocytes needs to be addressed in future intervention studies.

393 A previous study showed that Wnt/β-catenin signaling positively regulates *Mlxipl* and DNL
394 genes in white adipocytes, and that ChREBP functions downstream of Wnt signaling [76]. The
395 strong enrichment of Wnt signaling in lipogenic versus other adipocyte subtypes observed in
396 our study suggests that this pathway is also important in brown adipocytes, contributing to the
397 establishment of the lipogenic adipocyte identity via ChREBP. Specifically, *Wnt5a* and *Wnt5b*
398 isoforms – capable of signaling through both canonical pathways and non-canonical Wnt
399 pathways (Wnt5a [77]; Wnt5b [78]) – exhibited the strongest association with lipogenic

adipocytes. Furthermore, our cell-cell interaction analysis indicates that these signals predominantly originate from slow or fast muscle fibers and stroma-derived adipocyte progenitors, suggesting a coordinated multicellular regulatory network. In line with this, Lundgren *et al.* reported a preferential spatial association of lipogenic adipocytes with non-adipocyte cell types, supporting a role for local instructive cues. Notably, the loss of lipogenic adipocytes and ChREBP in our knockout model was accompanied by a decoupling of Wnt signaling and lipogenic adipocyte identity, raising the possibility that ChREBP itself may participate in a positive feedback loop that enhances Wnt pathway activity, thereby stabilizing the lipogenic phenotype. The recent identification of distinct futile-cycle-driven adipocyte subpopulations in WAT [79] also supports the idea that transcriptional and functional plasticity in thermogenic adipose tissues is governed by tightly regulated intercellular communication networks. Taken together, these data suggest that Wnt-ChREBP crosstalk not only establishes but potentially maintains lipogenic adipocyte identity within the BAT, embedded in a broader tissue-wide communication network essential for BAT plasticity and adaptation. Another important finding of the current study was that BAT-specific ChREBP knockout mice displayed unaltered energy expenditure under cold conditions. These findings are consistent with a recent paper reporting cold tolerance of ChREBP deficient mice [80] and show that BAT DNL in general is not essential for adaptive thermogenesis, which may be explained by compensatory lipid uptake from exogenous sources [31]. Of note, the strong drop in lipogenic adipocyte number after one day of cold exposure apparently does not affect thermogenesis, showing that the lipogenic adipocytes *per se* are also not indispensable for heat generation. In this context, one has to keep in mind that other adipocytes, in particular, the basal adipocytes, have in aggregate a greater contribution to DNL gene expression even at room temperature and this contribution increases upon cold exposure. Also in other metabolic pathways, we observed only partial enrichment of metabolic pathways and futile cycles within adipocyte subpopulations. This appears to be in contrast to WAT. DNL-high adipocytes could be clearly distinguished from lipid-uptake-high adipocytes [81] and fatty acid oxidation-high adipocytes [82] in epididymal and inguinal depots, respectively. Another study identified two distinct beige adipocyte subtypes in inguinal WAT, one high in futile cycling, the other high in *Ucp1* [79]. Similarly, beige adipocytes high in creatine cycling could be distinguished from such high in *Ucp1* [83]. These observations support the notion that murine BAT contains a highly adaptable pool of adipocytes whose functional states, including lipogenic capacity, can be rapidly adjusted to thermogenic demand, without strict dependency on specific subpopulations.

In conclusion, our study provides a comprehensive single-nucleus transcriptomic map of the murine BAT and highlights the remarkable plasticity of its adipocyte subtypes during cold adaptation. We show that BAT function is robustly maintained despite dynamic shifts in the composition and metabolic specialization of adipocyte populations, including the near-

437 complete loss of lipogenic adipocytes in ChREBP-deficient BAT. The identification of Wnt-
438 ChREBP cross-talk as a key determinant of lipogenic adipocyte identity adds an important
439 piece to the puzzle of how the BAT integrates local signals to fine-tune its thermogenic and
440 anabolic functions. Furthermore, our results highlight fundamental differences between brown
441 and white adipose tissue, as BAT thermogenesis appears to be less dependent on fixed,
442 metabolically distinct adipocyte subtypes compared to WAT. Future studies should address
443 whether similar plasticity exists in human BAT and whether targeting intercellular pathways,
444 such as Wnt signaling, may offer therapeutic strategies to modulate BAT function in metabolic
445 diseases.

446

447 ## 4. MATERIAL AND METHODS

448 ### 4.1. Mice

449 Mouse studies were approved by the Institutional Animal Care and Use Committee at the
450 University Medical Center Hamburg-Eppendorf. Age- (12 to 20 weeks) and weight-matched
451 male ChREBPα-flox-Ucp1 Cre mice [31] were housed at room temperature (22°C) or at cold
452 (6°C) for either 24 hours or 10 days at a 12h light/12h dark cycle with *ad libitum* access to
453 water and food (chow diet, Altromin). For organ harvest, mice were anesthetized with ketamine
454 (180 mg/kg) / xylazine (24 mg/kg), and systemically perfused with PBS via the left heart
455 ventricle. Interscapular BAT was excised and snap-frozen in liquid nitrogen.

456 ### 4.2. Isolation of nuclei from mice BAT

457 Adipocyte nuclei were isolated following a modified nuclear isolation protocol [79]. Frozen
458 adipose tissue was minced into 1–3 mm pieces on ice. The minced tissue was homogenized
459 in a Dounce homogenizer on ice in 0.1% CHAPS in CST buffer with 0.2U Rnase inhibitor, lysed
460 for 5 min, and quenched by 1% BSA in PBS with 0.2U Rnase inhibitor. The homogenized
461 adipose tissue was filtered through a 40 µm cell strainer and centrifuged at 500 x g for 5 min
462 at 4°C. The pellet was resuspended and washed with 1% BSA in PBS with 0.2U Rnase
463 inhibitor. The nuclei suspension was centrifuged again at 500 x g for 5 min at 4°C,
464 resuspended in 1% BSA containing PBS with 1U Rnase inhibitor, and filtered through a 20 µm
465 strainers. Nuclei were loaded on a 10x Chip G directly.

466 ### 4.3. snRNA-seq analysis

467 10X-libraries were prepared with the Chromium Single Cell V3.1 reagent kit following the
468 manufacturer's protocol (10X Genomics). Nuclei suspensions containing around 1200 nuclei
469 per µL were loaded into Chip G followed by reverse transcription to obtain cDNA. The cDNA

470 was amplified and used for library construction. Libraries were sequenced by Novogene using
471 partial lanes on an Illumina platform.

472 **4.4. RNA isolation, cDNA synthesis and qRT-PCR**

473 Tissues were homogenized in 1 ml of TRIzol reagent (ThermoFisher) using a TissueLyser type
474 3 (QIAGEN; 20 Hz for 2×3min). 250 µL chloroform was added, samples were mixed and
475 centrifuged. Supernatant was added to 600 µL of 70% ethanol. Further purification was
476 performed by using NucleoSpin RNAII Kit (Machery&Nagel) according to the manufacturer's
477 instructions. Double-stranded DNA was digested using rDNase I (kit). 400 ng purified RNA
478 were used for cDNA synthesis using High-Capacity cDNA Archive Kit (ThermoFisher) and
479 reverse transcription PCR program was as followed: 1. 10 min, 25°C; 2. 120 min, 37°C; 3.5 s,
480 85°C. Gene expression was assessed using Taqman assays supplied as assays-on-demands
481 (AoDs, ThermoFisher): Tbp (00446973_m1), *Mlxipl*_exon1a-2 = *Mlxipl* isoform 1 (Chrebpα)
482 (01196407_m1), *Fasn* (00662319_m1), *Acaca* (Mm01304285_m), *Tshr* (Mm00442027_m1),
483 *Slc2a3* (Mm00441483_m1).

484 **4.5. Western blotting**

485 Tissues were homogenized in 10x (v/w) RIPA buffer (50 mM Tris-HCl pH 7.4; 5 mM EDTA;
486 150 mM NaCl; 1 mM Na-pyrophosphate; 1 mM NaF; 1 mM Na-vanadate; 1% NP-40)
487 supplemented with complete Mini protease inhibitor (Roche) using TissueLyser-type3
488 (QIAGEN; 20 Hz for 2×3min). Samples were centrifuged and supernatant was collected
489 without upper lipid layer contamination. Protein was quantified by bicinchoninic acid assay
490 (BCA). Sample concentration was adjusted with RIPA buffer and 2-fold NuPAGE® LDS
491 Sample buffer + Sample Reducing Agent (Invitrogen) was added. 20µg of total protein were
492 separated in 10% Tris-glycine SDS-PAGE and transfered to nitrocellulose membranes (GE
493 healthcare) in a wet blotting system (blotting buffer: 20 mM Tris, 150 mM glycine, 20% (v/v)
494 methanol) overnight at 200 mA. Membranes were stained with Ponceau Red (Sigma), cut and
495 blocked for 1 h in 5% milk in TBS-T (20 mM Tris, 150 mM NaCl, 0.1% (v/v) Tween 20).
496 Membranes were incubated overnight at 4°C in the corresponding primary antibodies diluted
497 1:1000 in 5% BSA (Sigma) in TBS-T. After washing in TBS-T, membranes were incubated for
498 1 hour at RT in the corresponding HRP-conjugated secondary antibody diluted 1:5000 in 5%
499 milk in TBS-T. After washing in TBS-T, detection was performed with Amersham Imager 600
500 (GE healthcare) using SuperSignal West Femto ECL (Thermofisher). Primary antibodies: ACC
501 (Cell Signalling, #3662), FASN (BD Biosciences, #610962. HRP-conjugated secondary
502 antibodies: α-mouse (Jackson, #115-035-146,), α-rabbit (Jackson, #111-03-144).

503 **4.6. Fatty acid determination GC-MS**

504 Fatty acid composition in total lipid extracts of ~15 mg iBAT was determined by gas
505 chromatography. Method was adapted from Schlein *et al*. [31]. In brief, tissues were
506 homogenized in a 50-fold (v/w) volume of 2:1 chloroform/methanol [84] using TissueLyser-
507 type3 (QIAGEN; 20 Hz for 2×3min). Phase separation was achieved by centrifugation (15 min,
508 13.000 g, 4 °C) and upper layer (lipid extract) was collected. Derivatisation was performed with
509 100 µl lipid extract, 1 mL 4:1 methanol/toluene and 100 µl internal standard mix (hepatdecanoic
510 acid, tetradecanoate d27 and heptadecanoate d33, 200µg/ml each in methanol/toluene 4/1).
511 100 µl acetyl chloride were added while mixing and capped tubes were incubated at 100 °C
512 for 1 hour. After cooling to room temperature, 3 mL of 6% sodium carbonate was added for
513 neutralization. The mixture was centrifuged (1,800 g, 5 min) and ~200 µL of the upper layer
514 was transferred into auto sampler vials. Gas chromatography analyses were performed using
515 Trace 1310 gas chromatograph (Thermo Fisher) employed with following stationary phase:
516 DB-225 30m x 0.25mm i.d., film thickness 0.25 µm (Agilent) a mass spectrometer (ISQ 7000
517 GC-MS, ThermoFisher Scientific, Dreieich, Germany) respectively. Peak identification and
518 quantification were performed by comparing retention times and peak areas, respectively, to
519 standard chromatograms and internal standards. All calculations are based on fatty acid
520 methyl ester values.

521 **4.7. Indirect calorimetry**

522 For indirect calorimetry, mice were acclimated to metabolic cages (Promethion®, Sable
523 Systems) at 22°C for 2 days. Afterwards, ambient temperature was decreased to 6°C. Oxygen
524 consumption, carbon dioxide production, food and water intake were monitored continuously
525 for 10 days. The data files were analyzed according to the manufacturer (Sable Systems) using
526 the Macro interpreter software. RQ was calculated as $V(CO_2)/V(O_2)$.

527 **4.8. Data analysis and statistics**

528 Single-nucleus mRNA-sequencing (snRNA-seq) data were processed using the Seurat [85]
529 package (v5.1) in R. For quality control, nuclei with more than 15% mitochondrial reads, more
530 than 25,000 mRNA counts or more than 5,000 detected features were excluded. Upon quality
531 control, the data were log-normalised using Seurat's NormalizeData function. Six samples
532 were integrated using the Harmony algorithm [86] and resulted in a combined dataset of 36,611
533 nuclei and 22,992 features. Clusters were determined based on the top 30 principal
534 components with a 'resolution' = 0.8, yielding a total of 22 clusters. To identify cluster-specific
535 marker genes, differential expression analysis was performed using the FindAllMarkers
536 function, focusing on positive markers with a minimum expression fraction of 25%. Based on
537 these marker genes, clusters were annotated in a semi-supervised manner, with two individual
538 clusters being assigned to basal brown adipocytes. RNA velocity was modelled using the
539 scVelo (v0.3.3) pipeline [87]. Following preprocessing, RNA velocity was estimated using the

stochastic model, and velocity vectors were projected onto the UMAP embedding computed in Seurat. Pathway scores were calculatedPathway activity inference was performed using PROGENy (v1.28.0; [69]). The top 500 most informative genes were used to compute PROGENy scores, which were normalized by Z-score scaling across cell types. Cell-cell communication analysis was performed using LIANA (v0.1.14; [70]), which is a consensus resource for ligand-receptor interactions. The analysis was adapted for murine genes and interactions were ranked using the SCA and NATMI methods.

Unless indicated otherwise, group comparisons were performed by non-parametric Mann-Whitney U test, with correction for multiple testing (when applicable), * $p < 0.05$; ** $p < 0.01$; *** $p < 0.001$.

CREDIT AUTHORSHIP CONTRIBUTION STATEMENT

Janina Behrens: Writing - review & editing, Writing - original draft, Methodology, Investigation, Formal analysis, Data curation, Conceptualization. **Tongtong Wang:** Writing - review & editing, Methodology, Investigation. **Christoph Kilian:** Writing - review & editing, Data curation, Data analysis. **Anna Worthmann:** Writing - review & editing, Methodology. **Joerg Heeren:** Writing - review & editing, Funding acquisition, Conceptualization. **Lorenz Adlung:** Writing - review & editing, Writing - original draft, Data curation, Data analysis, Conceptualization. **Ludger Scheja:** Writing - review & editing, Writing - original draft, Data analysis, Supervision, Funding acquisition, Conceptualization.

DECLARATION OF COMPETING INTEREST

The authors declare that they have no known competing financial interests or personal relationships that could have appeared to influence the work reported in this paper.

ACKNOWLEDGMENTS

The authors thank Vivian Ruscheck, Laura Ehlen and Meike Kröger for excellent technical assistance. Ludger Scheja, Anna Worthmann and Joerg Heeren were supported by funds of the Deutsche Forschungsgemeinschaft DFG (450149205-TRR333/1). Christoph Kilian is supported by the iDfellows Hamburg Clinician Scientist Programme in Infectious Diseases (DFG, 493624519). Lorenz Adlung is supported by funding from the DFG (528292361), and the Klaus Tschira Boost Fund, a joint initiative of the German Scholars Organization and the Klaus Tschira Foundation.

DATA AVAILABILITY

All scripts and data objects required to reproduce the results of the snRNA-seq analysis will be freely available upon publication at: https://github.com/AdlungLab/ChREBP.

REFERENCES

[1] Cannon, B., Nedergaard, J., 2004. Brown adipose tissue: function and physiological significance. Physiological Reviews 84(1): 277–359, Doi: 10.1152/physrev.00015.2003.

[2] Nicholls, D.G., 2021. Mitochondrial proton leaks and uncoupling proteins. Biochimica Et Biophysica Acta. Bioenergetics 1862(7): 148428, Doi: 10.1016/j.bbabio.2021.148428.

[3] Chouchani, E.T., Kazak, L., Spiegelman, B.M., 2019. New Advances in Adaptive Thermogenesis: UCP1 and Beyond. Cell Metabolism 29(1): 27–37, Doi: 10.1016/j.cmet.2018.11.002.

[4] Rahbani, J.F., Roesler, A., Hussain, M.F., Samborska, B., Dykstra, C.B., Tsai, L., et al., 2021. Creatine kinase B controls futile creatine cycling in thermogenic fat. Nature 590(7846): 480–5, Doi: 10.1038/s41586-021-03221-y.

[5] Rahbani, J.F., Bunk, J., Lagarde, D., Samborska, B., Roesler, A., Xiao, H., et al., 2024. Parallel control of cold-triggered adipocyte thermogenesis by UCP1 and CKB. Cell Metabolism 36(3): 526-540.e7, Doi: 10.1016/j.cmet.2024.01.001.

[6] Bartness, T.J., Ryu, V., 2015. Neural control of white, beige and brown adipocytes. International Journal of Obesity Supplements 5(Suppl 1): S35-39, Doi: 10.1038/ijosup.2015.9.

[7] Braun, K., Oeckl, J., Westermeier, J., Li, Y., Klingenspor, M., 2018. Non-adrenergic control of lipolysis and thermogenesis in adipose tissues. The Journal of Experimental Biology 221(Pt Suppl 1): jeb165381, Doi: 10.1242/jeb.165381.

[8] Mottillo, E.P., Bloch, A.E., Leff, T., Granneman, J.G., 2012. Lipolytic products activate peroxisome proliferator-activated receptor (PPAR) α and δ in brown adipocytes to match fatty acid oxidation with supply. The Journal of Biological Chemistry 287(30): 25038–48, Doi: 10.1074/jbc.M112.374041.

[9] Mouisel, E., Bodon, A., Noll, C., Cassant-Sourdy, S., Marques, M.-A., Flores-Flores, R., et al., 2025. Cold-induced thermogenesis requires neutral-lipase-mediated intracellular lipolysis in brown adipocytes. Cell Metabolism 37(2): 429-440.e5, Doi: 10.1016/j.cmet.2024.10.018.

[10] Fedorenko, A., Lishko, P.V., Kirichok, Y., 2012. Mechanism of fatty-acid-dependent UCP1 uncoupling in brown fat mitochondria. Cell 151(2): 400–13, Doi: 10.1016/j.cell.2012.09.010.

[11] Bartelt, A., Bruns, O.T., Reimer, R., Hohenberg, H., Ittrich, H., Peldschus, K., et al., 2011. Brown adipose tissue activity controls triglyceride clearance. Nature Medicine 17(2): 200–5, Doi: 10.1038/nm.2297.

[12] Simcox, J., Geoghegan, G., Maschek, J.A., Bensard, C.L., Pasquali, M., Miao, R., et al., 2017. Global Analysis of Plasma Lipids Identifies Liver-Derived Acylcarnitines as a Fuel Source for Brown Fat Thermogenesis. Cell Metabolism 26(3): 509-522.e6, Doi: 10.1016/j.cmet.2017.08.006.

[13] Heine, M., Fischer, A.W., Schlein, C., Jung, C., Straub, L.G., Gottschling, K., et al., 2018. Lipolysis Triggers a Systemic Insulin Response Essential for Efficient Energy Replenishment of Activated Brown Adipose Tissue in Mice. Cell Metabolism 28(4): 644-655.e4, Doi: 10.1016/j.cmet.2018.06.020.

[14] Stanford, K.I., Middelbeek, R.J.W., Townsend, K.L., An, D., Nygaard, E.B., Hitchcox, K.M., et al., 2013. Brown adipose tissue regulates glucose homeostasis and insulin sensitivity. The Journal of Clinical Investigation 123(1): 215–23, Doi: 10.1172/JCI62308.

[15] Yoneshiro, T., Wang, Q., Tajima, K., Matsushita, M., Maki, H., Igarashi, K., et al., 2019. BCAA catabolism in brown fat controls energy homeostasis through SLC25A44. Nature 572(7771): 614–9, Doi: 10.1038/s41586-019-1503-x.
[16] Park, G., Haley, J.A., Le, J., Jung, S.M., Fitzgibbons, T.P., Korobkina, E.D., et al., 2023. Quantitative analysis of metabolic fluxes in brown fat and skeletal muscle during thermogenesis. Nature Metabolism 5(7): 1204–20, Doi: 10.1038/s42255-023-00825-8.
[17] Sanchez-Gurmaches, J., Tang, Y., Jespersen, N.Z., Wallace, M., Martinez Calejman, C., Gujja, S., et al., 2018. Brown Fat AKT2 Is a Cold-Induced Kinase that Stimulates ChREBP-Mediated De Novo Lipogenesis to Optimize Fuel Storage and Thermogenesis. Cell Metabolism 27(1): 195-209.e6, Doi: 10.1016/j.cmet.2017.10.008.
[18] Mottillo, E.P., Balasubramanian, P., Lee, Y.-H., Weng, C., Kershaw, E.E., Granneman, J.G., 2014. Coupling of lipolysis and de novo lipogenesis in brown, beige, and white adipose tissues during chronic β3-adrenergic receptor activation. Journal of Lipid Research 55(11): 2276–86, Doi: 10.1194/jlr.M050005.
[19] Jung, S.M., Doxsey, W.G., Le, J., Haley, J.A., Mazuecos, L., Luciano, A.K., et al., 2021. In vivo isotope tracing reveals the versatility of glucose as a brown adipose tissue substrate. Cell Reports 36(4): 109459, Doi: 10.1016/j.celrep.2021.109459.
[20] Trayhurn, P., 1979. Fatty acid synthesis in vivo in brown adipose tissue, liver and white adipose tissue of the cold-acclimated rat. FEBS Letters 104(1): 13–6, Doi: 10.1016/0014-5793(79)81075-3.
[21] Xue, Y., Petrovic, N., Cao, R., Larsson, O., Lim, S., Chen, S., et al., 2009. Hypoxia-independent angiogenesis in adipose tissues during cold acclimation. Cell Metabolism 9(1): 99–109, Doi: 10.1016/j.cmet.2008.11.009.
[22] Puigserver, P., Wu, Z., Park, C.W., Graves, R., Wright, M., Spiegelman, B.M., 1998. A cold-inducible coactivator of nuclear receptors linked to adaptive thermogenesis. Cell 92(6): 829–39, Doi: 10.1016/s0092-8674(00)81410-5.
[23] Cattaneo, P., Mukherjee, D., Spinozzi, S., Zhang, L., Larcher, V., Stallcup, W.B., et al., 2020. Parallel Lineage-Tracing Studies Establish Fibroblasts as the Prevailing In Vivo Adipocyte Progenitor. Cell Reports 30(2): 571-582.e2, Doi: 10.1016/j.celrep.2019.12.046.
[24] Lee, Y.-H., Petkova, A.P., Konkar, A.A., Granneman, J.G., 2015. Cellular origins of cold-induced brown adipocytes in adult mice. FASEB Journal: Official Publication of the Federation of American Societies for Experimental Biology 29(1): 286–99, Doi: 10.1096/fj.14-263038.
[25] Burl, R.B., Rondini, E.A., Wei, H., Pique-Regi, R., Granneman, J.G., 2022. Deconstructing cold-induced brown adipocyte neogenesis in mice. eLife 11: e80167, Doi: 10.7554/eLife.80167.
[26] Shamsi, F., Piper, M., Ho, L.-L., Huang, T.L., Gupta, A., Streets, A., et al., 2021. Vascular smooth muscle-derived Trpv1+ progenitors are a source of cold-induced thermogenic adipocytes. Nature Metabolism 3(4): 485–95, Doi: 10.1038/s42255-021-00373-z.
[27] Tran, K.-V., Gealekman, O., Frontini, A., Zingaretti, M.C., Morroni, M., Giordano, A., et al., 2012. The vascular endothelium of the adipose tissue gives rise to both white and brown fat cells. Cell Metabolism 15(2): 222–9, Doi: 10.1016/j.cmet.2012.01.008.

[28] Lundgren, P., Sharma, P.V., Dohnalová, L., Coleman, K., Uhr, G.T., Kircher, S., et al., 2023. A subpopulation of lipogenic brown adipocytes drives thermogenic memory. Nature Metabolism, Doi: 10.1038/s42255-023-00893-w.
[29] Jois, T., Chen, W., Howard, V., Harvey, R., Youngs, K., Thalmann, C., et al., 2017. Deletion of hepatic carbohydrate response element binding protein (ChREBP) impairs glucose homeostasis and hepatic insulin sensitivity in mice. Molecular Metabolism 6(11): 1381–94, Doi: 10.1016/j.molmet.2017.07.006.
[30] Kong, X., Banks, A., Liu, T., Kazak, L., Rao, R.R., Cohen, P., et al., 2014. IRF4 is a key thermogenic transcriptional partner of PGC-1α. Cell 158(1): 69–83, Doi: 10.1016/j.cell.2014.04.049.
[31] Schlein, C., Fischer, A.W., Sass, F., Worthmann, A., Tödter, K., Jaeckstein, M.Y., et al., 2021. Endogenous Fatty Acid Synthesis Drives Brown Adipose Tissue Involution. Cell Reports 34(2): 108624, Doi: 10.1016/j.celrep.2020.108624.
[32] Moser, C., Straub, L.G., Rachamin, Y., Dapito, D.H., Kulenkampff, E., Ding, L., et al., 2021. Quantification of adipocyte numbers following adipose tissue remodeling. Cell Reports 35(4): 109023, Doi: 10.1016/j.celrep.2021.109023.
[33] Herman, M.A., Peroni, O.D., Villoria, J., Schön, M.R., Abumrad, N.A., Blüher, M., et al., 2012. A novel ChREBP isoform in adipose tissue regulates systemic glucose metabolism. Nature 484(7394): 333–8, Doi: 10.1038/nature10986.
[34] Sun, W., Dong, H., Balaz, M., Slyper, M., Drokhlyansky, E., Colleluori, G., et al., 2020. snRNA-seq reveals a subpopulation of adipocytes that regulates thermogenesis. Nature 587(7832): 98–102, Doi: 10.1038/s41586-020-2856-x.
[35] Perdikari, A., Leparc, G.G., Balaz, M., Pires, N.D., Lidell, M.E., Sun, W., et al., 2018. BATLAS: Deconvoluting Brown Adipose Tissue. Cell Reports 25(3): 784-797.e4, Doi: 10.1016/j.celrep.2018.09.044.
[36] Seale, P., Kajimura, S., Yang, W., Chin, S., Rohas, L.M., Uldry, M., et al., 2007. Transcriptional control of brown fat determination by PRDM16. Cell Metabolism 6(1): 38–54, Doi: 10.1016/j.cmet.2007.06.001.
[37] Ahmadian, M., Liu, S., Reilly, S.M., Hah, N., Fan, W., Yoshihara, E., et al., 2018. ERRγ Preserves Brown Fat Innate Thermogenic Activity. Cell Reports 22(11): 2849–59, Doi: 10.1016/j.celrep.2018.02.061.
[38] Müller, S., Perdikari, A., Dapito, D.H., Sun, W., Wollscheid, B., Balaz, M., et al., 2020. ESRRG and PERM1 Govern Mitochondrial Conversion in Brite/Beige Adipocyte Formation. Frontiers in Endocrinology 11: 387, Doi: 10.3389/fendo.2020.00387.
[39] Uldry, M., Yang, W., St-Pierre, J., Lin, J., Seale, P., Spiegelman, B.M., 2006. Complementary action of the PGC-1 coactivators in mitochondrial biogenesis and brown fat differentiation. Cell Metabolism 3(5): 333–41, Doi: 10.1016/j.cmet.2006.04.002.
[40] Zhou, Z., Yon Toh, S., Chen, Z., Guo, K., Ng, C.P., Ponniah, S., et al., 2003. Cidea-deficient mice have lean phenotype and are resistant to obesity. Nature Genetics 35(1): 49–56, Doi: 10.1038/ng1225.
[41] de Jesus, L.A., Carvalho, S.D., Ribeiro, M.O., Schneider, M., Kim, S.W., Harney, J.W., et al., 2001. The type 2 iodothyronine deiodinase is essential for adaptive thermogenesis in brown adipose tissue. The Journal of Clinical Investigation 108(9): 1379–85, Doi: 10.1172/JCI13803.
[42] Kanehisa, M., Furumichi, M., Sato, Y., Matsuura, Y., Ishiguro-Watanabe, M., 2025. KEGG: biological systems database as a model of the real world. Nucleic Acids Research 53(D1): D672–7, Doi: 10.1093/nar/gkae909.

[43] Ismail, A., Tanasova, M., 2022. Importance of GLUT Transporters in Disease Diagnosis and Treatment. International Journal of Molecular Sciences 23(15): 8698, Doi: 10.3390/ijms23158698.
[44] Suchacki, K.J., Tavares, A.A.S., Mattiucci, D., Scheller, E.L., Papanastasiou, G., Gray, C., et al., 2020. Bone marrow adipose tissue is a unique adipose subtype with distinct roles in glucose homeostasis. Nature Communications 11(1): 3097, Doi: 10.1038/s41467-020-16878-2.
[45] Martinez-deMena, R., Anedda, A., Cadenas, S., Obregon, M.-J., 2015. TSH effects on thermogenesis in rat brown adipocytes. Molecular and Cellular Endocrinology 404: 151–8, Doi: 10.1016/j.mce.2015.01.028.
[46] Endo, T., Kobayashi, T., 2008. Thyroid-stimulating hormone receptor in brown adipose tissue is involved in the regulation of thermogenesis. American Journal of Physiology. Endocrinology and Metabolism 295(2): E514-518, Doi: 10.1152/ajpendo.90433.2008.
[47] Lundbäck, V., Kulyté, A., Dahlman, I., Marcus, C., 2020. Adipose-specific inactivation of thyroid stimulating hormone receptors in mice modifies body weight, temperature and gene expression in adipocytes. Physiological Reports 8(16): e14538, Doi: 10.14814/phy2.14538.
[48] Liu, Q., Long, Q., Zhao, J., Wu, W., Lin, Z., Sun, W., et al., 2023. Cold-Induced Reprogramming of Subcutaneous White Adipose Tissue Assessed by Single-Cell and Single-Nucleus RNA Sequencing. Research (Washington, D.C.) 6: 0182, Doi: 10.34133/research.0182.
[49] Backman, K., Mears, W.E., Waheeb, A., Beaulieu Bergeron, M., McClintock, J., de Nanassy, J., et al., 2021. A splice site and copy number variant responsible for TTC25-related primary ciliary dyskinesia. European Journal of Medical Genetics 64(5): 104193, Doi: 10.1016/j.ejmg.2021.104193.
[50] Tharp, K.M., Kang, M.S., Timblin, G.A., Dempersmier, J., Dempsey, G.E., Zushin, P.-J.H., et al., 2018. Actomyosin-Mediated Tension Orchestrates Uncoupled Respiration in Adipose Tissues. Cell Metabolism 27(3): 602-615.e4, Doi: 10.1016/j.cmet.2018.02.005.
[51] Rasmussen, M., Jin, J.-P., 2021. Troponin Variants as Markers of Skeletal Muscle Health and Diseases. Frontiers in Physiology 12: 747214, Doi: 10.3389/fphys.2021.747214.
[52] Kim, M., Franke, V., Brandt, B., Lowenstein, E.D., Schöwel, V., Spuler, S., et al., 2020. Single-nucleus transcriptomics reveals functional compartmentalization in syncytial skeletal muscle cells. Nature Communications 11(1): 6375, Doi: 10.1038/s41467-020-20064-9.
[53] Song, W., Yang, Y., Heizer, P., Tu, Y., Weston, T.A., Kim, J.R., et al., 2023. Intracapillary LPL levels in brown adipose tissue, visualized with an antibody-based approach, are regulated by ANGPTL4 at thermoneutral temperatures. Proceedings of the National Academy of Sciences of the United States of America 120(8): e2219833120, Doi: 10.1073/pnas.2219833120.
[54] Son, N.-H., Basu, D., Samovski, D., Pietka, T.A., Peche, V.S., Willecke, F., et al., 2018. Endothelial cell CD36 optimizes tissue fatty acid uptake. The Journal of Clinical Investigation 128(10): 4329–42, Doi: 10.1172/JCI99315.
[55] Fischer, A.W., Jaeckstein, M.Y., Heeren, J., 2022. Lysosomal acid lipase promotes endothelial proliferation in cold-activated adipose tissue. Adipocyte 11(1): 28–33, Doi: 10.1080/21623945.2021.2013416.
[56] Iso, T., Maeda, K., Hanaoka, H., Suga, T., Goto, K., Syamsunarno, M.R.A.A., et al., 2013. Capillary endothelial fatty acid binding proteins 4 and 5 play a critical role in fatty acid uptake in heart and skeletal muscle. Arteriosclerosis,

Thrombosis, and Vascular Biology 33(11): 2549–57, Doi: 10.1161/ATVBAHA.113.301588.
[57] Inouye, K.E., Prentice, K.J., Lee, A., Wang, Z.B., Dominguez-Gonzalez, C., Chen, M.X., et al., 2023. Endothelial-derived FABP4 constitutes the majority of basal circulating hormone and regulates lipolysis-driven insulin secretion. JCI Insight 8(14): e164642, Doi: 10.1172/jci.insight.164642.
[58] Ekman, N., Lymboussaki, A., Västrik, I., Sarvas, K., Kaipainen, A., Alitalo, K., 1997. Bmx tyrosine kinase is specifically expressed in the endocardium and the endothelium of large arteries. Circulation 96(6): 1729–32, Doi: 10.1161/01.cir.96.6.1729.
[59] Kalucka, J., de Rooij, L.P.M.H., Goveia, J., Rohlenova, K., Dumas, S.J., Meta, E., et al., 2020. Single-Cell Transcriptome Atlas of Murine Endothelial Cells. Cell 180(4): 764-779.e20, Doi: 10.1016/j.cell.2020.01.015.
[60] Lee, H.-W., Xu, Y., He, L., Choi, W., Gonzalez, D., Jin, S.-W., et al., 2021. Role of Venous Endothelial Cells in Developmental and Pathologic Angiogenesis. Circulation 144(16): 1308–22, Doi: 10.1161/CIRCULATIONAHA.121.054071.
[61] Elmore, J.P., McGee, M.C., Nidetz, N.F., Anannya, O., Huang, W., August, A., 2020. Tuning T helper cell differentiation by ITK. Biochemical Society Transactions 48(1): 179–85, Doi: 10.1042/BST20190486.
[62] Liu, C., Raab, M., Gui, Y., Rudd, C.E., 2023. Multi-functional adaptor SKAP1: regulator of integrin activation, the stop-signal, and the proliferation of T cells. Frontiers in Immunology 14: 1192838, Doi: 10.3389/fimmu.2023.1192838.
[63] Yang, N., Zuchero, J.B., Ahlenius, H., Marro, S., Ng, Y.H., Vierbuchen, T., et al., 2013. Generation of oligodendroglial cells by direct lineage conversion. Nature Biotechnology 31(5): 434–9, Doi: 10.1038/nbt.2564.
[64] Chen, B., Banton, M.C., Singh, L., Parkinson, D.B., Dun, X.-P., 2021. Single Cell Transcriptome Data Analysis Defines the Heterogeneity of Peripheral Nerve Cells in Homeostasis and Regeneration. Frontiers in Cellular Neuroscience 15: 624826, Doi: 10.3389/fncel.2021.624826.
[65] Mecklenburg, J., Shein, S.A., Malmir, M., Hovhannisyan, A.H., Weldon, K., Zou, Y., et al., 2023. Transcriptional profiles of non-neuronal and immune cells in mouse trigeminal ganglia. Frontiers in Pain Research (Lausanne, Switzerland) 4: 1274811, Doi: 10.3389/fpain.2023.1274811.
[66] Agrawal, A., Balcı, H., Hanspers, K., Coort, S.L., Martens, M., Slenter, D.N., et al., 2024. WikiPathways 2024: next generation pathway database. Nucleic Acids Research 52(D1): D679–89, Doi: 10.1093/nar/gkad960.
[67] Lindquist, J.M., Rehnmark, S., 1998. Ambient temperature regulation of apoptosis in brown adipose tissue. Erk1/2 promotes norepinephrine-dependent cell survival. The Journal of Biological Chemistry 273(46): 30147–56, Doi: 10.1074/jbc.273.46.30147.
[68] La Manno, G., Soldatov, R., Zeisel, A., Braun, E., Hochgerner, H., Petukhov, V., et al., 2018. RNA velocity of single cells. Nature 560(7719): 494–8, Doi: 10.1038/s41586-018-0414-6.
[69] Schubert, M., Klinger, B., Klünemann, M., Sieber, A., Uhlitz, F., Sauer, S., et al., 2018. Perturbation-response genes reveal signaling footprints in cancer gene expression. Nature Communications 9(1): 20, Doi: 10.1038/s41467-017-02391-6.
[70] Dimitrov, D., Türei, D., Garrido-Rodriguez, M., Burmedi, P.L., Nagai, J.S., Boys, C., et al., 2022. Comparison of methods and resources for cell-cell communication inference from single-cell RNA-Seq data. Nature Communications 13(1): 3224, Doi: 10.1038/s41467-022-30755-0.

[71] Spaethling, J.M., Sanchez-Alavez, M., Lee, J., Xia, F.C., Dueck, H., Wang, W., et al., 2016. Single-cell transcriptomics and functional target validation of brown adipocytes show their complex roles in metabolic homeostasis. FASEB Journal: Official Publication of the Federation of American Societies for Experimental Biology 30(1): 81–92, Doi: 10.1096/fj.15-273797.
[72] Maniyadath, B., Zhang, Q., Gupta, R.K., Mandrup, S., 2023. Adipose tissue at single-cell resolution. Cell Metabolism 35(3): 386–413, Doi: 10.1016/j.cmet.2023.02.002.
[73] Wallmeier, J., Shiratori, H., Dougherty, G.W., Edelbusch, C., Hjeij, R., Loges, N.T., et al., 2016. TTC25 Deficiency Results in Defects of the Outer Dynein Arm Docking Machinery and Primary Ciliary Dyskinesia with Left-Right Body Asymmetry Randomization. American Journal of Human Genetics 99(2): 460–9, Doi: 10.1016/j.ajhg.2016.06.014.
[74] Backman, K., Mears, W.E., Waheeb, A., Beaulieu Bergeron, M., McClintock, J., de Nanassy, J., et al., 2021. A splice site and copy number variant responsible for TTC25-related primary ciliary dyskinesia. European Journal of Medical Genetics 64(5): 104193, Doi: 10.1016/j.ejmg.2021.104193.
[75] Hilgendorf, K.I., Johnson, C.T., Mezger, A., Rice, S.L., Norris, A.M., Demeter, J., et al., 2019. Omega-3 Fatty Acids Activate Ciliary FFAR4 to Control Adipogenesis. Cell 179(6): 1289-1305.e21, Doi: 10.1016/j.cell.2019.11.005.
[76] Bagchi, D.P., Nishii, A., Li, Z., DelProposto, J.B., Corsa, C.A., Mori, H., et al., 2020. Wnt/β-catenin signaling regulates adipose tissue lipogenesis and adipocyte-specific loss is rigorously defended by neighboring stromal-vascular cells. Molecular Metabolism 42: 101078, Doi: 10.1016/j.molmet.2020.101078.
[77] Rogers, S., Scholpp, S., 2022. Vertebrate Wnt5a - At the crossroads of cellular signalling. Seminars in Cell & Developmental Biology 125: 3–10, Doi: 10.1016/j.semcdb.2021.10.002.
[78] Perkins, R.S., Suthon, S., Miranda-Carboni, G.A., Krum, S.A., 2022. WNT5B in cellular signaling pathways. Seminars in Cell & Developmental Biology 125: 11–6, Doi: 10.1016/j.semcdb.2021.09.019.
[79] Wang, T., Sharma, A.K., Wu, C., Maushart, C.I., Ghosh, A., Yang, W., et al., 2024. Single-nucleus transcriptomics identifies separate classes of UCP1 and futile cycle adipocytes. Cell Metabolism 36(9): 2130-2145.e7, Doi: 10.1016/j.cmet.2024.07.005.
[80] Wei, C., Wang, P., Dong, Q., Ma, X.-H., Lu, M., Qi, S., et al., 2022. ChREBP-regulated lipogenesis is not required for the thermogenesis of brown adipose tissue. International Journal of Obesity (2005) 46(5): 1068–75, Doi: 10.1038/s41366-022-01082-7.
[81] Sárvári, A.K., Van Hauwaert, E.L., Markussen, L.K., Gammelmark, E., Marcher, A.-B., Ebbesen, M.F., et al., 2021. Plasticity of Epididymal Adipose Tissue in Response to Diet-Induced Obesity at Single-Nucleus Resolution. Cell Metabolism 33(2): 437-453.e5, Doi: 10.1016/j.cmet.2020.12.004.
[82] Lee, Y.-H., Kim, S.-N., Kwon, H.-J., Granneman, J.G., 2017. Metabolic heterogeneity of activated beige/brite adipocytes in inguinal adipose tissue. Scientific Reports 7: 39794, Doi: 10.1038/srep39794.
[83] Vargas-Castillo, A., Sun, Y., Smythers, A.L., Grauvogel, L., Dumesic, P.A., Emont, M.P., et al., 2024. Development of a functional beige fat cell line uncovers independent subclasses of cells expressing UCP1 and the futile creatine cycle. Cell Metabolism: S1550413124002730, Doi: 10.1016/j.cmet.2024.07.002.

[84] Folch, J., Ascoli, I., Lees, M., Meath, J.A., LeBARON, N., 1951. Preparation of lipide extracts from brain tissue. The Journal of Biological Chemistry 191(2): 833–41.
[85] Hao, Y., Stuart, T., Kowalski, M.H., Choudhary, S., Hoffman, P., Hartman, A., et al., 2024. Dictionary learning for integrative, multimodal and scalable single-cell analysis. Nature Biotechnology 42(2): 293–304, Doi: 10.1038/s41587-023-01767-y.
[86] Korsunsky, I., Millard, N., Fan, J., Slowikowski, K., Zhang, F., Wei, K., et al., 2019. Fast, sensitive and accurate integration of single-cell data with Harmony. Nature Methods 16(12): 1289–96, Doi: 10.1038/s41592-019-0619-0.
[87] Bergen, V., Lange, M., Peidli, S., Wolf, F.A., Theis, F.J., 2020. Generalizing RNA velocity to transient cell states through dynamical modeling. Nature Biotechnology 38(12): 1408–14, Doi: 10.1038/s41587-020-0591-3.

892 ## Figure Legends

893 **Figure 1: Identification of distinct clusters of adipocytes and other cell types in BAT by**
894 **snRNA-seq. A** mRNA expression of ChREBPα (*Mlxipl* isoform 1) and ChREBPβ (*Mlxipl*
895 isoform 2) measured by qPCR and **B** Western blot of ChREBP in iBAT from ChREBP-flox mice
896 (Cre-) and ChREBP-flox Ucp1-Cre (Cre+) mice housed at 22°C (RT) or at 6°C for one day
897 (acute cold, AC) or 10 days (chronic cold, CC). A: n=4, means ± SEM of Student's t-test, $*p <$
898 0.05, $**p < 0.01$, $***p < 0.001$. **C** UMAP of all 36,611 nuclei isolated from iBAT of 21 mice
899 including both genotypes (Cre-, Cre+) and all three housing conditions (RT, AC, CC). **D** Brown
900 and white adipocyte score (based on Perdikari *et al*., 2018, Supplemental Table 1), and **E**
901 Bubble plot of selected marker genes in Cre- mice housed at RT.

902 **Figure 2: *Ttc25* is a specific marker of lipogenic adipocytes strongly associated with**
903 **DNL and thermogenic metabolism. A** Pearson correlation of genes expressed in nuclei of
904 the lipogenic adipocytes found in this study (Cre-, CC) compared to those identified by
905 Lundgren *et al.* [28]. **B** Vulcano plot of genes expressed by lipogenic vs. basal adipocytes. **C**
906 Normalized expression of *Fasn* and *Ttc25* on UMAP (Cre-, RT). **D** Waterfall plot of genes
907 correlating with *Ttc25* across all lipogenic adipocytes (Cre-). **E** Gene ontology (GO) term
908 analysis (biological processes) of genes highly (i.e., r>0, p adj. < 0.001) correlating with *Ttc25*
909 in lipogenic adipocytes.

910 **Figure 3: Dynamic changes in adipocytes during cold adaptation. A** Relative frequencies
911 of adipocyte clusters from Cre- mice. **B** Normalized expression of metabolic pathway genes in
912 adipocytes from Cre- mice. Gene list in Supplemental Table 1. **C** Violin plot of apoptosis score
913 of white-like and lipogenic adipocytes from Cre- mice. Gene list in Supplemental Table 1. **D**
914 Fold change of aggregated expression of *Acaca* and *Fasn* from Cre- mice. **E** Fold change of
915 mRNA expression of *Acaca* and *Fasn* measured by qPCR in iBAT of Cre- mice. Mean ± SEM
916 of n = 4 mice per group. Student's t-test, $*p < 0.05$, $**p < 0.01$, $***p < 0.001$. **F** Aggregated
917 expression of *Acaca* and *Fasn* in adipocytes from Cre- mice. **G, H** RNA velocity vectors
918 projected on UMAP of scRNA-seq data for Cre- AC (**G**) and Cre- CC (**H**).

919 **Figure 4: Lipogenic adipocyte identity depends on ChREBP and is linked to Wnt**
920 **signaling. A** Fold change of mRNA expression of *Acaca* and *Fasn* measured by qPCR in
921 iBAT. Mean ± SEM of n = 4 mice per group. Student's t-test, $*p < 0.05$, $**p < 0.01$, $***p <$
922 0.001. **B** Western blot of ACC and FASN from iBAT. **C** Fold change of aggregated expression
923 of *Acaca* and *Fasn*. **D** Fatty acid quantification of 14:0 (myristic acid) and 16:0 (palmitic acid)
924 fatty acid from iBAT. Mean ± SEM of n = 4 mice per group. Student's t-test, $*p < 0.05$, $**p <$
925 0.01, $***p < 0.001$. **E** Frequency band of adipocytes. **F** Scaled PROGENy pathway scores
926 across adipocytes from all conditions (Cre-, Cre+, RT, AC, CC). **G** Boxplots of WNT PROGENy

927 score of lipogenic adipocytes. Nuclei of the three housing conditions were combined.
928 Wilcoxon-test, $*p < 0.05$, $**p < 0.01$, $***p < 0.001$. **H** Aggregated expression of Wnt ligands
929 in BAT from Cre- mice. **I** Cell-Cell-Interactions with lipogenic adipocytes as targets of Wnt
930 ligands. **J** Significant (i.e. corrected p value < 0.05) interactions between indicated cellular
931 subsets in BAT.

932

933 **Figure S1: Identification of cell types based on gene expression.** Unless indicated
934 otherwise, snRNA-seq data were used for the analysis shown in the graphs. **A** Violin plots of
935 normalized expression of indicated marker genes. **B** Normalized signature expression of
936 oxidative phosphorylation (OXPHOS) genes in the adipocyte subtypes. Data from Cre- mice
937 housed at RT. **C** mRNA expression of *Tshr* and *Slc2a3* measured by qPCR in iBAT, iWAT
938 (inguinal) and gWAT (gonadal) of Cre- mice housed at RT. Mean ±SEM. **D-G** Marker gene
939 expression in muscle fibers (**D**), endothelial cells and endothelium-derived adipocytes (**E**),
940 stromal cells and stroma-derived adipocytes (**F**) and other cell types (**G**) of Cre- mice at RT.

941 **Figure S2: Relative frequencies of the annotated cell types of BAT from Cre- mice.**

942 **Figure S3. DNL gene expression in presence and absence of ChREBP.** Normalized
943 snRNA-seq data from all conditions (RT, AC, CC) were combined to compare Cre- with Cre+
944 mice.

945 **Figure S4. Thermogenic gene expression and energy expenditure in presence and**
946 **absence of ChREBP. A** Violin plots of brown adipocyte score (based on Perdikari *et al.*)
947 Wilcoxon test, fdr-correction, $*p < 0.05$, $**p < 0.01$, $***p < 0.001$. **B** Oxygen consumption rate
948 (VO_2 in ml/min) measured by indirect calorimetry of Cre- and Cre+ mice. **C** Pearson correlation
949 between WNT PROGENy score and brown adipocyte score in lipogenic adipocytes of Cre-
950 and Cre+ mice. Nuclei of the three housing conditions were combined. snRNA-seq data were
951 used for **A** and **C**.

952

953

Figure 1

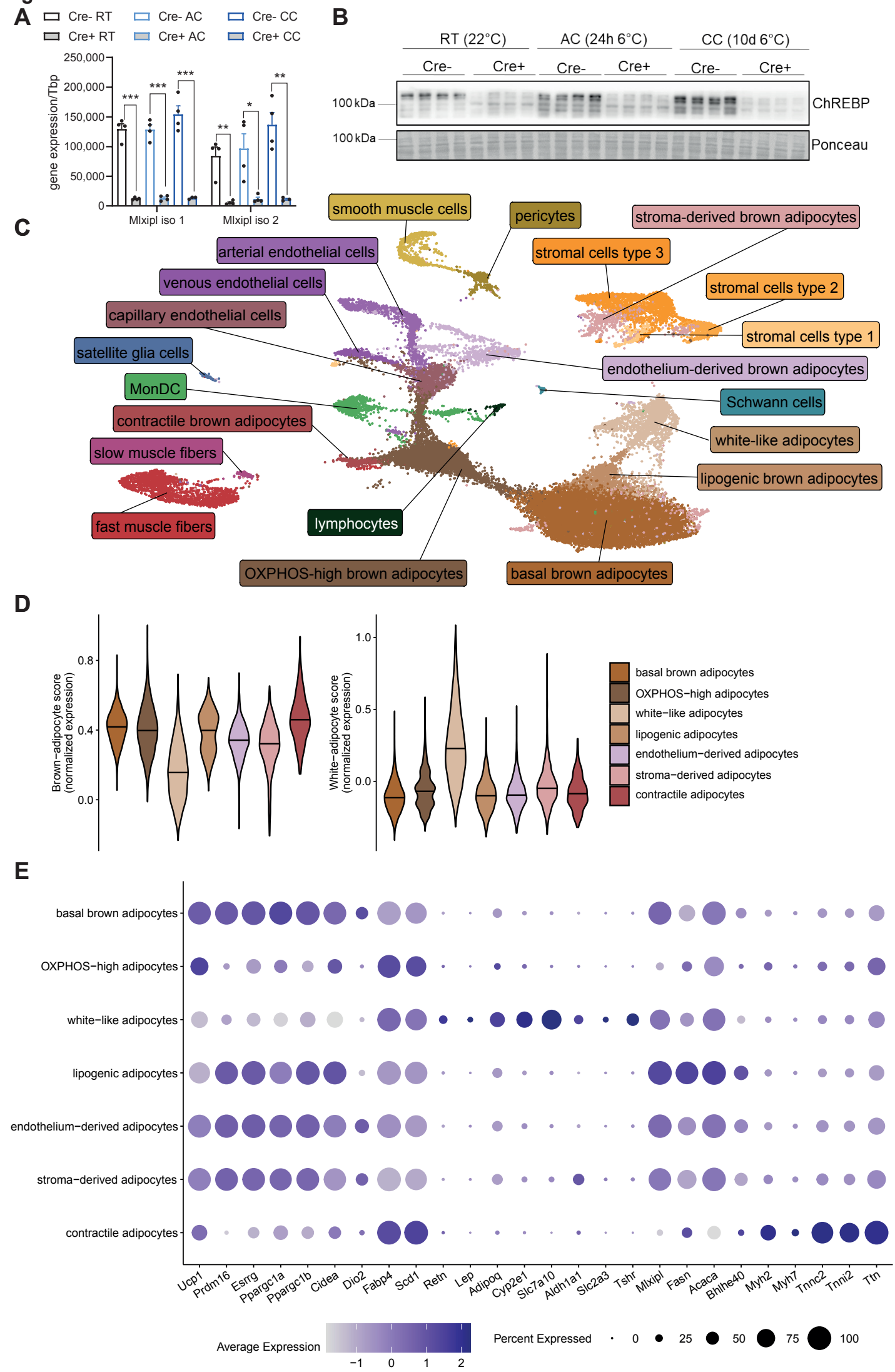
A
Cre- RT
Cre+ RT
Cre- AC
Cre+ AC
Cre- CC
Cre+ CC
gene expression/Tbp
250,000
200,000
150,000
100,000
50,000
0
***
***
***
**
*
**
Mlxipl iso 1
Mlxipl iso 2
B
RT (22°C)
AC (24h 6°C)
CC (10d 6°C)
Cre-
Cre+
Cre-
Cre+
Cre-
Cre+
100 kDa
ChREBP
100 kDa
Ponceau
C
smooth muscle cells
pericytes
stroma-derived brown adipocytes
arterial endothelial cells
stromal cells type 3
venous endothelial cells
stromal cells type 2
capillary endothelial cells
stromal cells type 1
satellite glia cells
endothelium-derived brown adipocytes
MonDC
Schwann cells
contractile brown adipocytes
white-like adipocytes
slow muscle fibers
lipogenic brown adipocytes
fast muscle fibers
lymphocytes
OXPHOS-high brown adipocytes
basal brown adipocytes
D
Brown-adipocyte score (normalized expression)
0.8
0.4
0.0
White-adipocyte score (normalized expression)
1.0
0.5
0.0
basal brown adipocytes
OXPHOS-high adipocytes
white-like adipocytes
lipogenic adipocytes
endothelium-derived adipocytes
stroma-derived adipocytes
contractile adipocytes
E
basal brown adipocytes
OXPHOS-high adipocytes
white-like adipocytes
lipogenic adipocytes
endothelium-derived adipocytes
stroma-derived adipocytes
contractile adipocytes
Ucp1
Prdm16
Esrrg
Ppargc1a
Ppargc1b
Cidea
Dio2
Fabp4
Scd1
Retn
Lep
Adipoq
Cyp2e1
Slc7a10
Aldh1a1
Slc2a3
Tshr
Mlxipl
Fasn
Acaca
Bhlhe40
Myh2
Myh7
Tnnc2
Tnni2
Ttn
Average Expression
−1
0
1
2
Percent Expressed
0
25
50
75
100

Figure 2

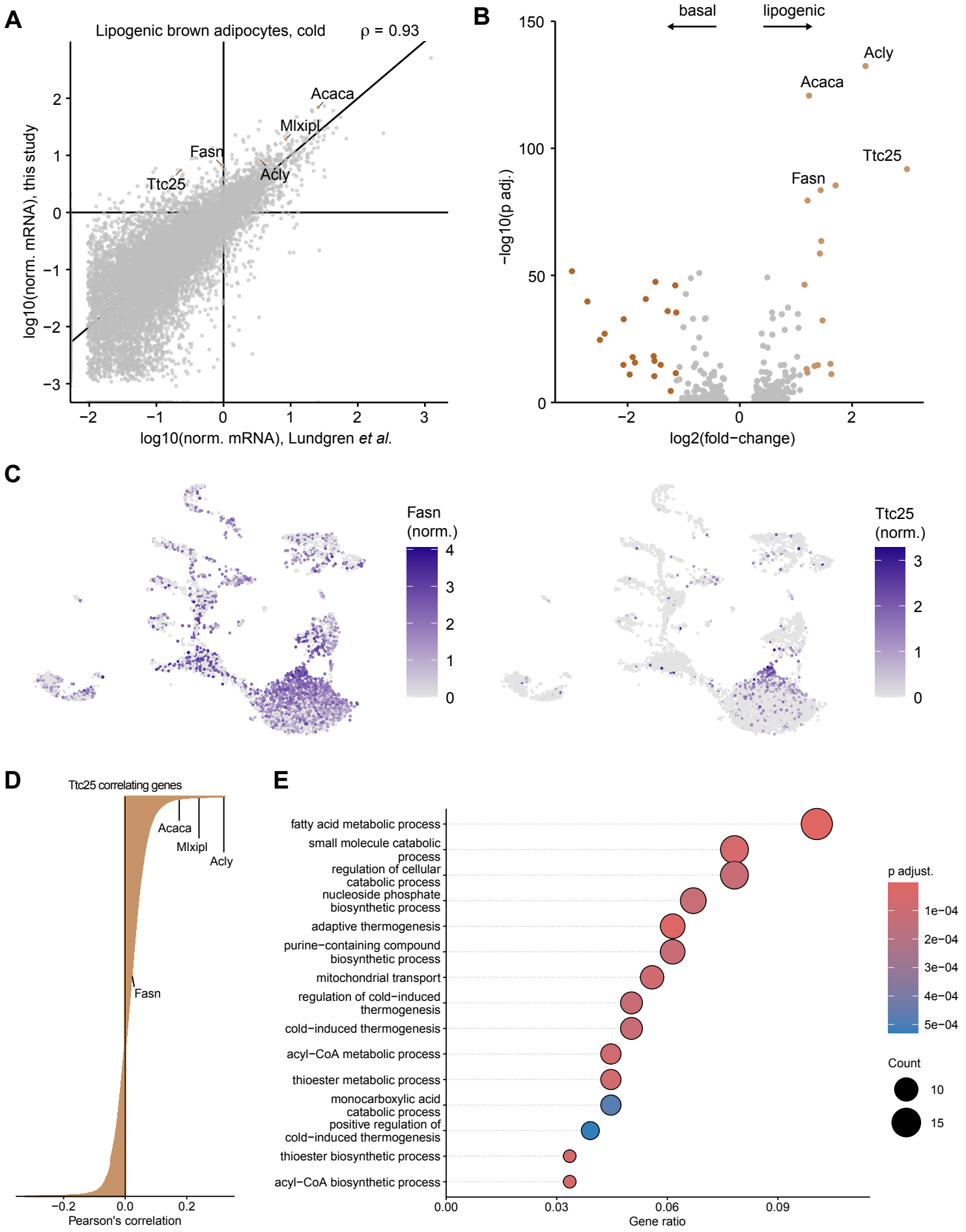
A
Lipogenic brown adipocytes, cold
ρ = 0.93
Acaca
Mlxipl
Fasn
Acly
Ttc25
log10(norm. mRNA), this study
log10(norm. mRNA), Lundgren et al.
B
basal
lipogenic
Acly
Acaca
Ttc25
Fasn
−log10(p adj.)
log2(fold−change)
C
Fasn (norm.)
Ttc25 (norm.)
D
Ttc25 correlating genes
Acaca
Mlxipl
Acly
Fasn
Pearson's correlation
E
fatty acid metabolic process
small molecule catabolic process
regulation of cellular catabolic process
nucleoside phosphate biosynthetic process
adaptive thermogenesis
purine−containing compound biosynthetic process
mitochondrial transport
regulation of cold−induced thermogenesis
cold−induced thermogenesis
acyl−CoA metabolic process
thioester metabolic process
monocarboxylic acid catabolic process
positive regulation of cold−induced thermogenesis
thioester biosynthetic process
acyl−CoA biosynthetic process
Gene ratio
p adjust.
Count

Figure 3

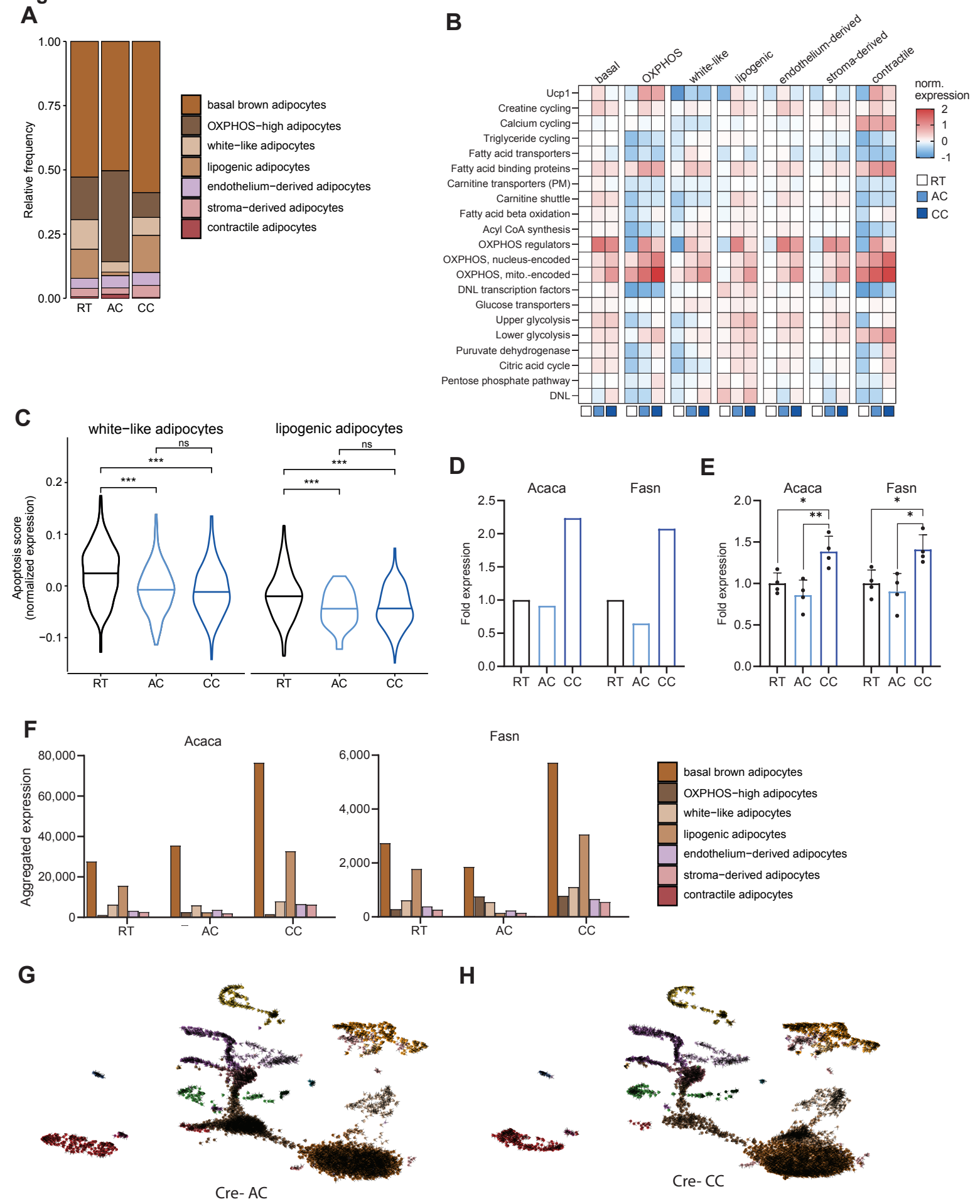
A
Relative frequency
1.00
0.75
0.50
0.25
0.00
RT
AC
CC
basal brown adipocytes
OXPHOS−high adipocytes
white−like adipocytes
lipogenic adipocytes
endothelium−derived adipocytes
stroma−derived adipocytes
contractile adipocytes
B
basal
OXPHOS
white-like
lipogenic
endothelium-derived
stroma-derived
contractile
Ucp1
Creatine cycling
Calcium cycling
Triglyceride cycling
Fatty acid transporters
Fatty acid binding proteins
Carnitine transporters (PM)
Carnitine shuttle
Fatty acid beta oxidation
Acyl CoA synthesis
OXPHOS regulators
OXPHOS, nucleus-encoded
OXPHOS, mito.-encoded
DNL transcription factors
Glucose transporters
Upper glycolysis
Lower glycolysis
Puruvate dehydrogenase
Citric acid cycle
Pentose phosphate pathway
DNL
norm. expression
2
1
0
-1
RT
AC
CC
C
white−like adipocytes
lipogenic adipocytes
Apoptosis score (normalized expression)
0.2
0.1
0.0
−0.1
***
***
ns
***
***
ns
RT
AC
CC
D
Acaca
Fasn
Fold expression
2.5
2.0
1.5
1.0
0.5
0.0
RT
AC
CC
E
Acaca
Fasn
Fold expression
2.0
1.5
1.0
0.5
0.0
*
**
*
*
RT
AC
CC
F
Acaca
Fasn
Aggregated expression
80,000
60,000
40,000
20,000
0
6,000
4,000
2,000
0
RT
AC
CC
basal brown adipocytes
OXPHOS−high adipocytes
white−like adipocytes
lipogenic adipocytes
endothelium−derived adipocytes
stroma−derived adipocytes
contractile adipocytes
G
Cre- AC
H
Cre- CC

Figure 4

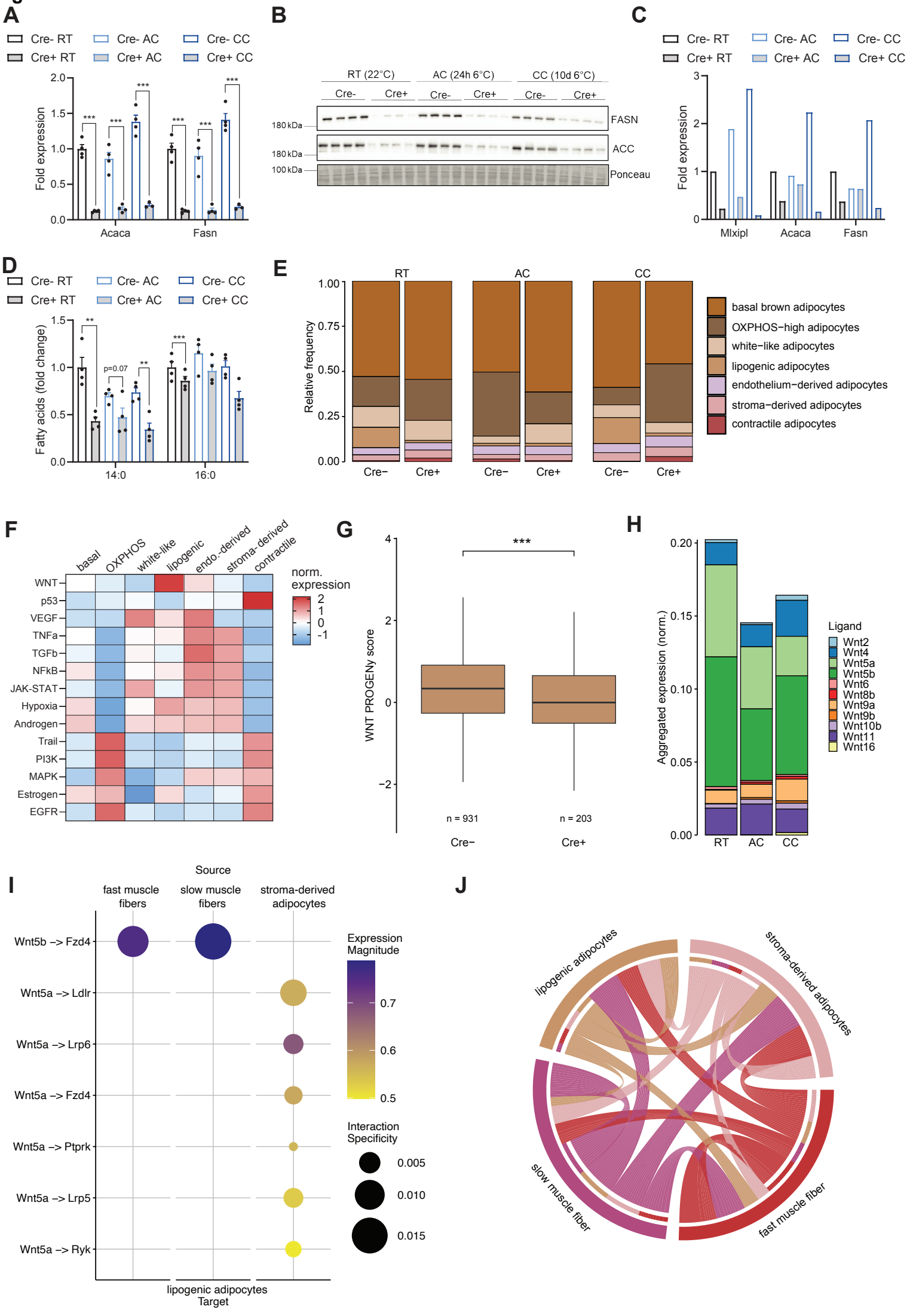
A
Cre- RT
Cre+ RT
Cre- AC
Cre+ AC
Cre- CC
Cre+ CC
Fold expression
Acaca
Fasn
B
RT (22°C)
AC (24h 6°C)
CC (10d 6°C)
Cre-
Cre+
180 kDa
100 kDa
FASN
ACC
Ponceau
C
Mlxipl
D
Fatty acids (fold change)
14:0
16:0
p=0.07
E
RT
AC
CC
Relative frequency
basal brown adipocytes
OXPHOS−high adipocytes
white−like adipocytes
lipogenic adipocytes
endothelium−derived adipocytes
stroma−derived adipocytes
contractile adipocytes
F
basal
OXPHOS
white-like
lipogenic
endo.-derived
stroma-derived
contractile
WNT
p53
VEGF
TNFa
TGFb
NFkB
JAK-STAT
Hypoxia
Androgen
Trail
PI3K
MAPK
Estrogen
EGFR
norm. expression
G
WNT PROGENy score
n = 931
n = 203
Cre−
Cre+
H
Aggregated expression (norm.)
Ligand
Wnt2
Wnt4
Wnt5a
Wnt5b
Wnt6
Wnt8b
Wnt9a
Wnt9b
Wnt10b
Wnt11
Wnt16
I
Source
fast muscle fibers
slow muscle fibers
stroma-derived adipocytes
Wnt5b –> Fzd4
Wnt5a –> Ldlr
Wnt5a –> Lrp6
Wnt5a –> Fzd4
Wnt5a –> Ptprk
Wnt5a –> Lrp5
Wnt5a –> Ryk
Expression Magnitude
Interaction Specificity
lipogenic adipocytes
Target
J
lipogenic adipocytes
stroma-derived adipocytes
slow muscle fiber
fast muscle fiber